SAND2015-10863C

Evaluation of Power Flow Control for an All-Electric Warship Power System with Pulsed Load Applications

J. Neely, *Member IEEE*, L. Rashkin, *Member, IEEE*, M. Cook, D. Wilson, *Member, IEEE*, S. Glover, *Senior Member, IEEE*
Sandia National Laboratories
Albuquerque, NM, USA
jneely@sandia.gov

***Abstract*— Future U.S. Navy ships will require power systems that meet more stringent agility, efficiency, scalability, controllability and resiliency requirements. Modularity and the ability to interconnect power systems having their own energy storage, generation, and loads is an enabling capability. To aid in the design of power system controls, much of what has been learned from advances in the control of networked microgrids is being applied. Developing alternative methods for controlling and analyzing these systems will provide insight into tradeoffs that can be made during the design phase. This paper considers the problem of electric ship power disturbances in response to pulsed loads, in particular, to electromagnetic launch systems. Recent literature has indicated that there exists a trade-off in information and power flow and that intelligent, coordinated control of power flow in a microgrid system (i.e. such as an electric ship) can modify energy storage hardware requirements. The control presented herein was developed to provide the necessary flexibility with little computational burden. It is described analytically and then demonstrated in simulation and hardware.**

Keywords—Navy all-electric ship, pulsed loads, power system stability, EMALS

I. INTRODUCTION

The all-electric warship provides the potential for unprecedented flexibility and system capability [1]. However, pulsed power launch, weapon and radar systems present design challenges [2]-[15]. Pulsed power subsystem integration is a technology challenge today and is a good motivating example for the development of a rational control approach for ship microgrids with information and power sharing. Numerous pulsed power studies have been conducted. Many focus on the bus voltage effects and methods for mitigation [5]. Some studies have postulated harmonizing pulsed power operation with other power intensive ship operations - typically the power plant of an electric ship [14]. Harmonizing all the ship's power assets through closed loop control has not been solved, but offers tremendous promise for enabling not only pulsed power technology, but also future technology with nonstandard power requirements.

Achieving regulation and power balance in a system with highly variable loads is a key capability addressed by this research. Specifically, a hierarchical networked microgrid control concept is being applied to the U.S. Navy's Electric Ship program. The controls approach is developed using a Hamiltonian-based power flow control methodology developed in [16]-[19] and expanded for use in electric ship power systems in [20]. Hamiltonian-based control allows for the kinetic and potential energy stored in the system state to be accounted for explicitly. In particular, since the control is applied herein to a DC-based system, the generators are not synchronized, and the power output of the generator is controlled through power electronics, allowing for some energy to be borrowed from the generator inertia and made available through high-bandwidth control. This can allow a reduction in the size of energy storage necessary but results in state disturbances, ie. greater generator speed deviations.

The control scheme has three layers including a guidance control, a Hamiltonian-based control and a servo control. The guidance control receives measurement information and computes changes to converter reference commands; these can be quasi-static (approx. 1 Hz) or rapid updates (approx.50-100 Hz). The Hamiltonian control is implemented herein as a proportional plus integral (PI) control. The servo control refers to the inner most control loop and pulse width modulation (PWM) scheme residing on each power converter; it operates on the fastest timescale to implement commands from the Hamiltonian control layer.

In this work, a notional electric ship reference model was generated using typical values from literature, the reference model was scaled to be represented using the Secure Scalable Microgrid testbed [21], and experiments were conducted to evaluate the use of hierarchical control. In particular, this work considers the implementation of a simple Guidance control scheme that adjusts power flow through filtering when pulsed loads are used. This scheme is an indirect way of affecting power flow but has a reduced computational burden compared to dynamic optimization planning schemes such as the one presented in [20]. The trade-off between energy storage and generator response is quantified in simulation and hardware.

The next section describes the microgrid testbed used for experimentation. Descriptions of the electric ship reference model and Electromagnetic Launch System (EMALS) pulsed load follow. Section IV reviews the Hamiltonian power flow control scheme. Section V describes the Guidance Control approach used in this study. Section VI provides simulation results for the notional system. Section VII provides

experimental results using the microgrid testbed. Finally, conclusions and discussion are provided in Section VIII.

II. Microgrid Testbed Description

The Secure Scalable MicroGrid Test Bed (SSMTB) was designed to conduct experiments on networked microgrids that share information flow and power flow [21]-[23]. The testbed includes three microgrid systems, a central bus cabinet for interconnecting the components, and computers used for control, data acquisition, and situational awareness. In total, the system components include: a reconfigurable bus cabinet, five permanent magnet generators, nine energy storage emulators capable of sourcing or sinking 5kW of power, seven 600V commercial power supplies, mechanical source emulators based on commercial motor drives, a DC/AC converter, a three-phase resistive load, three high-power digital resistors rated to 6.7 kW at 400V bus voltage, and a master control console that scripts the experiments with designated source and load profiles. Some key components are shown in Fig. 1. An example screenshot of the master control software is shown in Fig. 2 highlighting the coordination of several components and monitoring of several quantities for each scripted experiment. Additional information may be found in [20]-[23].

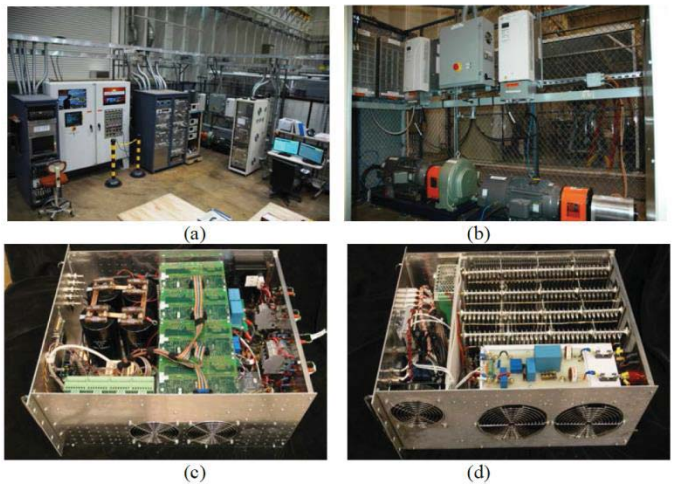

Fig. 1. Photos of (a) the microgrid testbed including (b) mechanical source emulators, (c) energy storage emulator, and (d) high power digital resistor

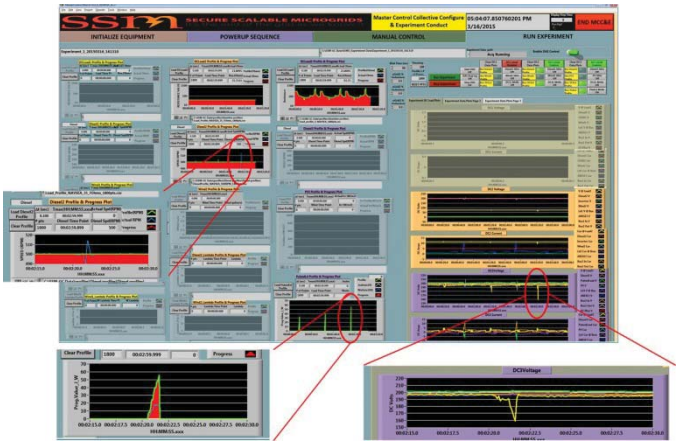

Fig. 2. Shows screen capture for the Master control computer summarizing experiment profile and outcomes with (top center) bus 3 load profile (left) generator 2 speed transients, (bottom left) pulsed load current, (bottom right) dc bus voltage

III. Electric Ship Reference Model

A notional electric ship was developed based on typical power levels and architectures identified in open literature [1]-[15]. The notional system is depicted in Fig. 3a. This notional system uses a high-voltage DC bus, relies heavily on power electronic converters to provide flexible power flow control, and includes a network to enable communication. The system was scaled down and emulated using components in the SSMTB, shown in Fig. 3b, thus providing a laboratory scale model of a 3-zone electric ship networked power system. To evaluate the response of bus voltage, generator speed transients and energy storage effort in response to an EMALS launch, the EMALs system was modeled and an emulator was built and integrated into the testbed.

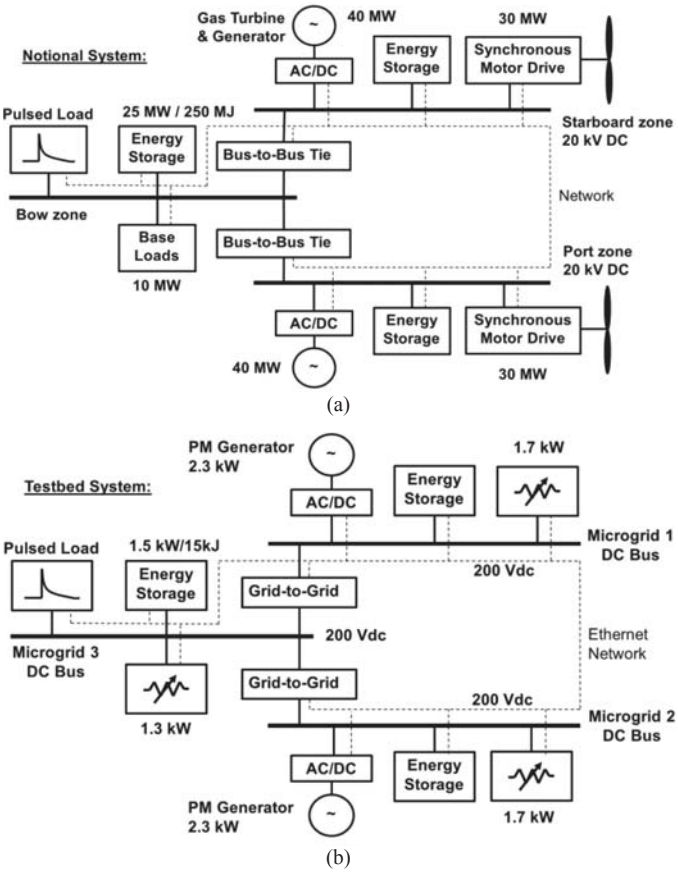

Fig. 3. Illustrates the development of a candidate (a) notional electric ship architecture and (b) possible hardware implementation using SSMTB components

A. Electromagnetic Launch System (EMALS)

The EMALS is a major component of the electric ship that will replace more conventional steam powered launch systems. The system must be capable of accelerating an aircraft to a launch speed of up to 103 m/s over the course of a ship's runway, approximately 73 m, [24] no matter the aircraft or how heavily loaded it is. Fig. 4 shows the expected application of force required of an EMALS system reported in [24] and the desired speed profile, which roughly scales with the square root of the position on the runway.

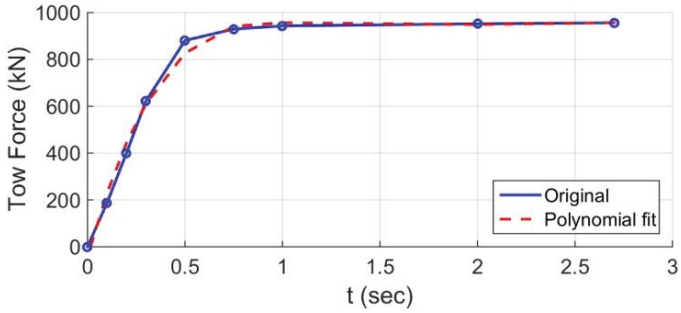

(a)

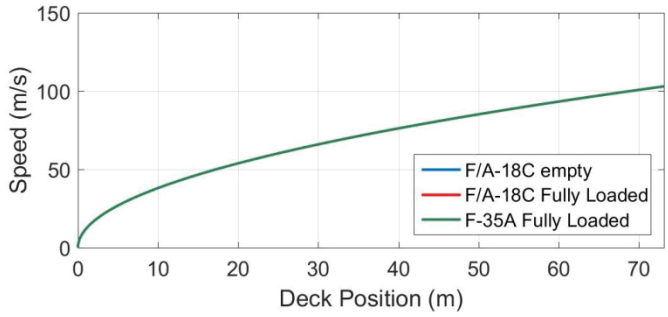

(b)

Fig. 4. Shows (top) EMALS force profile (from [24]) and (bottom) desired aircraft speed as a function of deck position

To accomplish this, a feedback controller was implemented to track the speed reference

$$v_{ref}(p) = v_{\max}\sqrt{\frac{p}{L}} \tag{1}$$

where p is the aircraft position on the runway, $v_{\max}$ is the final takeoff speed, and L is the effective length of the runway. The model also accounted for drag, but this was a small component of the force. The model was run for three different aircraft configurations and an end speed of 103 m/s: an unloaded F/A-18C with a mass of 10,400 kg, a fully loaded F/A-18C with a mass of 16,770 kg, and a fully loaded F-35A with a mass of 31,800 kg [25]-[26].

The resulting power expended on each aircraft configuration during a launch is shown in Fig. 5. This graph can be used to derive currents and voltages for modelling the behavior of the EMALS in the electrical system.

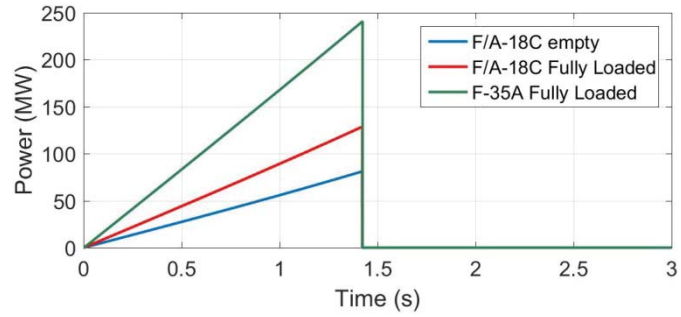

Fig. 5. Power output of EMALS system as a function of time for three different aircraft configurations assuming a take-off speed of 103 m/s

Assuming a relatively steady voltage, the power profile was emulated on the SSMTB using a custom pulsed load assembly that included several resistors connected in parallel through controlled semiconductor switches.

In addition to the EMALS load, the deck of the ship is a dynamic environment; the preparation, loading and movement of aircraft in advance of a launch requires electrical power and is assumed for the purposes of this study to have a similar profile surrounding each launch. Thus a baseload was also defined with a repeated profile.

IV. Power Flow Control Control Strategy

A nonlinear control design architecture based on *Hamiltonian Surface Shaping and Power Flow Control* (HSSPFC) has been employed [16],[27]. The HSSPFC scheme uses a power flow control approach that balances generation and dissipation subject to energy storage (kinetic and potential energies) which define the Hamiltonian for the system. Both static and dynamic stability conditions are determined. The model consists of three microgrid circuit models which are developed in references [20],[27]. Briefly, the model can be defined in matrix form as

$$M\dot{x} = Rx + v + u \tag{2}$$

where the M matrix consists of the passive energy storage elements (inductance, capacitance) of the circuit and the R matrix consists of the resistive elements of the circuit, and x is the system state. The v-vector consists of the general source inputs to the network and the u-vector contains the controller inputs. The u inputs are intended to be actuated by energy storage systems. The R matrix is decomposed further as the sum of a diagonal and skew-symmetric matrix components.

$$M\dot{x} = \left[\overline{R}(R_{load}) + \widetilde{R}(\lambda)\right]x + v + u \tag{3}$$

The vector x is composed of the system state (inductor currents, capacitor voltages). The error state along with the reference control are defined as

$$\Delta x = x_{ref} - x \tag{4}$$

It is assumed that the reference state vector is constant with $\dot{x}_{ref} = 0$, e.g., operating at some desired steady-state condition, and the reference control signal becomes

$$u_{ref} = -\left[\overline{R} + \widetilde{R}\right]x_{ref} - v \quad . \tag{5}$$

This steady-state reference relationship forms the basis from which the feedforward or guidance control stategy is discussed in the next section. Next, based on the error-state the Hamiltonian or energy surface is defined as

$$H = \frac{1}{2}\Delta x^T M \Delta x + \frac{1}{2}\left(\int \Delta x(t)dt\right)^T K_I \left(\int \Delta x(t)dt\right) \quad \forall \Delta x = 0 \tag{6}$$

where the controller integral term provides a control potential energy to help design or shape the energy surface to meet the static stability condition. Note the integral controller diagonal gain matrix K_I is positive definite.

The Hamiltonian time derivative (or power flow) becomes:

$$\dot{H} = \Delta x^T \overline{R} \Delta x + \Delta x^T \Delta u + \Delta x^T K_I \int \Delta x(t) dt \qquad (7)$$

where the skew-symmetric portion of the *R* matrix is zero and the feedback controller is determined by

$$\Delta u = u_{ref} - u \,. \qquad (8)$$

In the next step, a Proportional-Integral (PI) controller is proposed as

$$\Delta u = -K_P \Delta x - K_I \int \Delta x(t) dt \,. \qquad (9)$$

Substituting and simplifying the Hamiltonian time derivative (power flow) yields

$$\dot{H} = -\Delta x^T \left[K_P - \overline{R} \right] \Delta x < 0 \qquad (10)$$

which is the dynamic stability condition. Performance is determined by the selection of the proportional controller diagonal gain matrix K_P, defined as positive definite. The PI feedback controller designs have been integrated into the energy storage systems and the controller gains selected to provide the desired transient performances. The state model formulation in this work is similar to that provided in [20].

V. Guidance Control Strategy

The guidance controller provides regular updates to the power converters in the system. The generators and energy storage communicate current and voltage measurements as well as state-of-charge (SOC) estimates. The guidance controller sends voltage references to the energy storage units which then regulate bus voltage and their own SOC. The guidance controller also sends power commands to the converters that connect generators to the bus. Power requirements are computed using a realtime load estimator, voltage setpoints and energy storage SOC values.

Since the load is assumed to be purely resistive and all bus voltages are set to the same reference value, the load estimator estimates instantaneous load admittance based on bus currents and voltages transmitted to the guidance controller as

$$\hat{G}_{load} \cong N \frac{\sum_{i=1}^{N} \hat{i}_{b,i}}{\sum_{i=1}^{N} \hat{v}_{b,i}} \qquad (11)$$

where $i_{b,i}$ is output current into the bus and $v_{b,i}$ is the output voltage at the bus connection of the i^{th} component, *N* is the number of components, and the hatted quantities denote measured values. The estimated power required by the resistive load is thus

$$\hat{P}_{load} \cong \left(V_b^* \right)^2 \hat{G}'_{load} \qquad (12)$$

where V_b^* is the bus voltage setpoint and $\hat{G}'_{load}$ is the filtered load admittance estimate. The total commanded power, P_{tot}^*, is computed by summing the load power requirement, $\hat{P}_{load}$, and the desired charge/discharge power, P_{ES}^*, needed by the various energy storage resources, expressed as

$$P_{tot}^* = \hat{P}_{load} + P_{ES}^* \,. \qquad (13)$$

The duty-cycles and commanded currents are computed for the DC-DC boost converters using

$$\lambda_i^* = \frac{1}{2V_b^*} \left(\hat{v}_{si} + \sqrt{\hat{v}_{si}^2 - 4 r_{Li} \alpha_i \left(P_{tot}^* \right)} \right) \qquad (14)$$

$$i_{Li}^* = \frac{\alpha_i \left(P_{tot}^* \right)}{\lambda_i^* V_b^*} \qquad (15)$$

where λ_i^* is the "right-hand side" duty cycle of the boost converter (the duty cycle of the *top* switch), $\hat{v}_{si}$ is the measured boost converter input voltage, r_{Li} is the boost converter input resistance, and i_{Li}^* is the commanded boost converter input current. The converter then uses the Hamiltonian control to regulate $i_{Li} \to i_{Li}^*$.

The Guidance Control is depicted in Fig. 6. For the sake of brevity and clarity, we assumed $P_{ES}^* = 0$ in this work, and the SOC management is not applied in the simulation and experimental results herein; however, the signal is still included among the feedback signals shown in Fig. 6 and is expected to be part of future work.

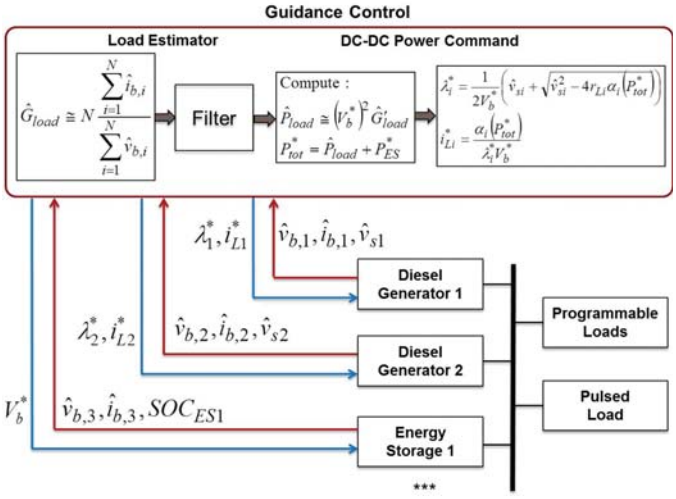

Fig. 6. Illustration of the guidance control strategy

VI. Simulation Results

Simulink simulation was performed on the scaled system in Fig. 3b. The simulations used a first-order continuous-time filter to regulate response of the AC/DC converters connecting diesel generators to the bus. It is noted that although gas turbine models would be preferable in this application, these were not available at the time; so, diesel generator models were used [21]. The system was tested in five simulation experiments with filter time constants of (1) 0.1356, (2) 0.5299, (3) 2.005, (4) 7.512, and (5) 28.56 seconds.

Each simulation experiment ran for 180 seconds. The SSMTB model buses 1 and 2 each had a constant resistance

load and a diesel engine with governor set to 950 RPM, the energy storage units regulated bus voltage using Hamiltonian-based control, and power flow through the bus-to-bus converters was controlled based on the AC/DC converter command and relative bus voltage errors. The pulsed load on Microgrid 3 (Bow zone) was varied to represent three simulated EMALS launches; the pulsed load was engaged at t = 20 sec for the F/A-18C empty case, then at t=80 sec for the F/A-18C fully loaded case, and finally at t=140 sec for the F-35A fully loaded case. An additional base load on Microgrid 3 was varied to simulate ancillary electrical systems that support each launch and thus repeated three times. See the bus 3 power profile in Fig. 7.

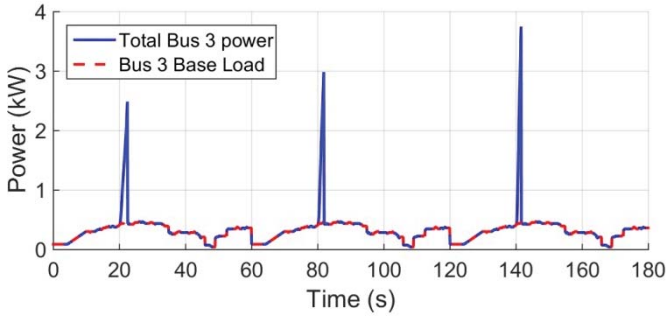

Fig. 7. The bow (Microgrid 3) load profile including the variable bus load and pulsed loads from simulated EMALS launches, scaled down for the SSMTB

In general, when the diesel generator converter output was bandwidth limited, the energy storage units that shared a bus with generation provided more control energy to mitigate high-frequency voltage disturbances which also resulted in a mitigation of generator speed disturbances. Fig. 8 shows the simulated bus currents (positive into the bus) from all the generator converters, energy storage converters, and the pulsed load. The figure shows that the filter does effect the response from the diesel generator converters and the port and starboard energy storage converters as expected. With a smaller time constant, the diesel generators are able to respond more quickly to the pulsed load. With a larger time constant the diesel generator responds to changes more slowly, and the pulsed load must be supplied by the energy storage units that respond to bus voltage error. It is noted that the energy storage responses are greatest in the case with the longest time constant: bow energy storage has a peak value of 5.65 A, and port/starboard energy storages have a peak of 8.11 A. In the case of the shortest time constant, bow energy storage has a peak value of 4.24 A and port/starboard units have a peak value of 1.71 A. The trade-off between generator and energy storage control energies is greatest when they share a bus or are electrically close since the energy storage is responding to bus voltage deviations.

Fig. 9 shows the generator speeds, relative to their 950 RPM reference, for the largest and smallest time constants. For the shortest time constant the generator speeds dip to 917, 913 and 909 RPM. For the 28.56 second time constant, there is far less variation with dips to about 948 RPM for each. This shows that the filter time constant has an appreciable effect on generator speed response.

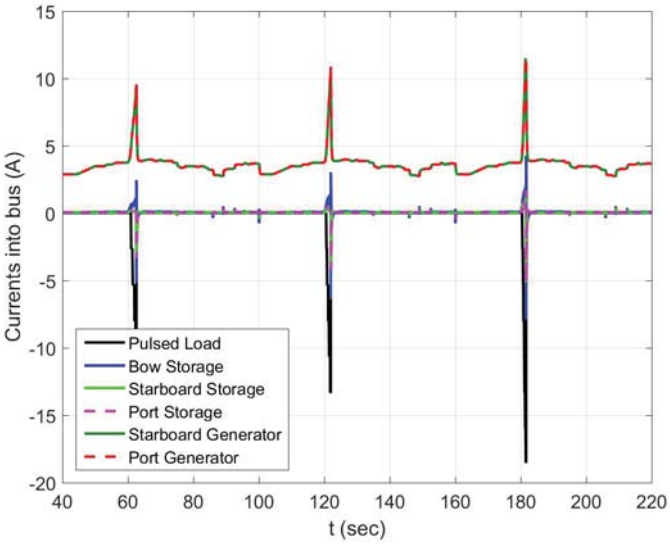

(a)

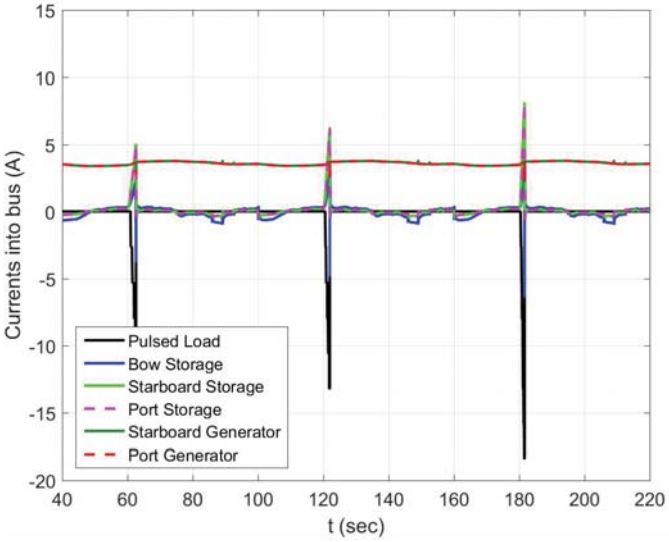

(b)

Fig. 8. Shows bus currents from generator-sourced converters and the energy storage emulator for (a) a time constant of 0.1356 seconds and (b) a time constant of 28.56 seconds.

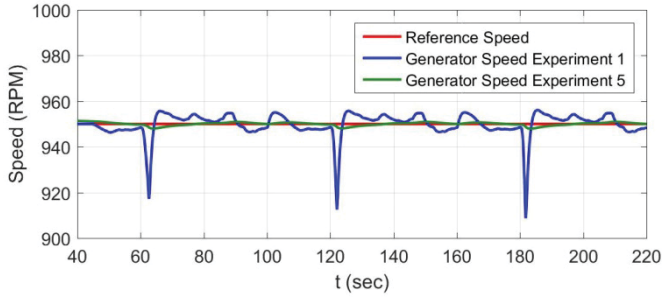

Fig. 9. Shows the speed of the starboard generator as compared to the reference speed for Experiment 1Experiment 5.

A. Design Trade-off

To help quantify the affect of the filter time constant on performance, a Pareto frontier was identified to investigate the

tradeoff between energy storage and generator control effort; the two performance quantities J_1 and J_2 are defined as

$$J_1 = \int_{t_0}^{t_f} \left(\sum_i^{N_{Gens}} \left(i_{bi}(\tau) - \hat{i}_{bi} \right)^2 \right) d\tau \quad (16)$$

$$J_2 = \int_{t_0}^{t_f} \left(\sum_i^{N_{ES}} \left(i_{ESi}(\tau) - \hat{i}_{ESi} \right)^2 \right) d\tau \quad (17)$$

where $i_{bi}(t)$ are the currents delivered to the respective busses by the starboard and port generator converters as a function of time, N_{Gens} is the number of generators, $i_{ESi}(t)$ are the bus currents from the N_{ES} energy storage systems, and the hatted quantities represent average currents over the interval $t \in \lfloor t_0, t_f \rfloor$ and are constant in (16) and (17). Fig. 10 shows the Pareto frontier between generator control effort and energy storage control effort for the simulated system with two generators and three energy storage systems. There is a clear trade-off between the two values with a mostly linear relationship.

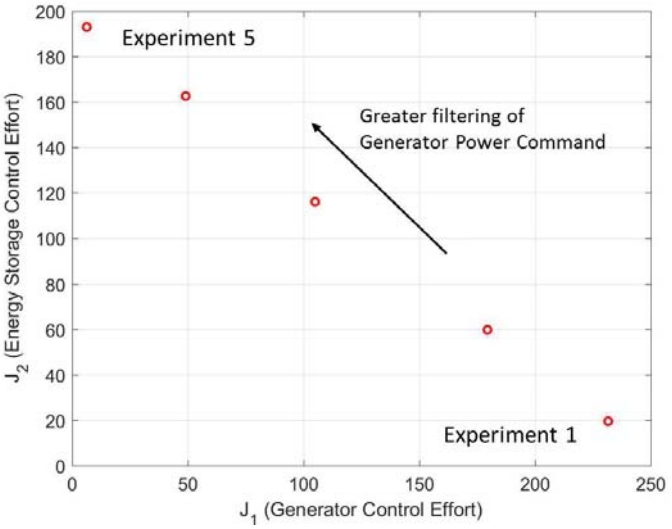

Fig. 10. Simulated trade space (Pareto Frontier) illustrating trade-off between generator control effort and energy storage control effort

VII. Experimental Results

As in simulation, the control was evaluated in a series of five hardware experiments that utilized select components from the testbed system in Fig. 3b at a reduced voltage of 150 V and generator speed of 650 RPM. The system configuration used for the hardware experiments is illustrated in Fig. 11. This system had fewer components than what was modeled in the simulation, but the results are consistent.

A. Experiment Description

As with the simulation, each experiment ran for 180 seconds with both generators engaged, the propulsion load represented as a constant resistance, the variable load on Microgrid 3 (Bow zone) was varied according to a predesignated profile to represent three simulated EMALS launches and a varying base load was implemented on the SSMTB bus 3. The power profile shown in Fig. 7 was used to program the pulsed load and programmable load. In each experiment, the generator converter power command was filtered by a digital low-pass filter with different equivalent time constants, corresponding to those used in simulation, before being transmitted to the generators by the Guidance controller. In experiment 1, the fast response of the power electronics effectively supplied the pulse energy by extracting that energy from the generator inertia, and the energy storage control effort was minimized. Experiment 5 had the lowest cut-off frequency; in this case, the generators provide a more averaged power, and the pulsed load is supplied primarily by the energy storage system. In this way, the control effort priority could be selected by the user and regulated by the Guidance controller through simple separation of time scales.

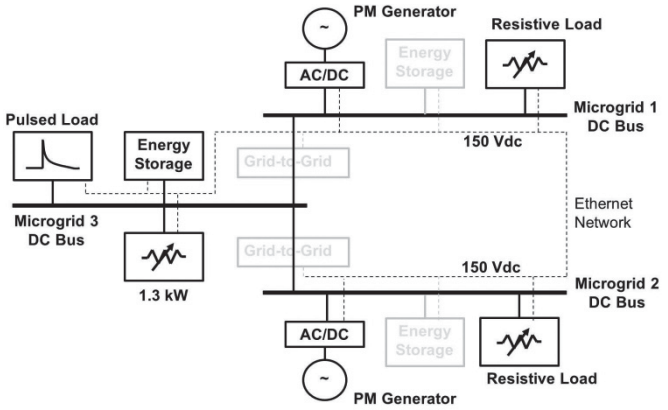

Fig. 11. Illustration of the dispatch control strategy used controlling the diesel generators. The faded components were not connected.

B. Experimental Results

Fig. 12 illustrates the component currents and bus voltages. Fig 12a shows the two generator currents, the energy storage current and the pulsed load current for Experiment 1. Therein, it is noted that the energy storage current is minimal, providing some current for the base load and when the pulsed load is active. The majority of the baseload power and pulsed load are tracked by the generators, which effectively comes from energy stored in the generator inertia since the speed governor operates at a much slower timescale. Fig 12b illustrates the Experiment 5 results; therein, the generator currents vary slowly, and the baseload and pulsed power demands are tracked by the energy storage. Fig. 12c shows the bus voltage, indicating that the system achieves very good voltage regulation despite the highly variable load. This is due to the fact that the energy storage directly regulates bus voltage; this is achievable because the guidance control system coordinates the energy resources rather than relying on droop control to balance the contributions from different generators. Both voltages have a mean of 148 V. The worst-case voltage deviation occurs for the 0.1356 sec time constant; the voltage spikes to 156.3 V (5.6% error) and immediately returns to steady state within 125 msec.

Fig. 13 shows generator speed transients (blue traces) relative to the speed reference (green traces) for Experiments 1 and 5 respectively. Therein, it is noted that the Experiment 1 case results in greater deviation in generator speed during a transient, including nadirs of 631 RPM, 620 RPM and 618 RPM, or 2.9%, 4.6% and 4.9% deviation. In addition, some variation is seen in the generator speed due to the variable baseload. As the load reference used to command generator power is filtered, the energy storage provides a greater share of the pulsed power, resulting in less generator deviation. Fig. 13b shows the generator speed nadirs at 642, 642, and 637 RPM respectively, with less variation seen due to base load as well.

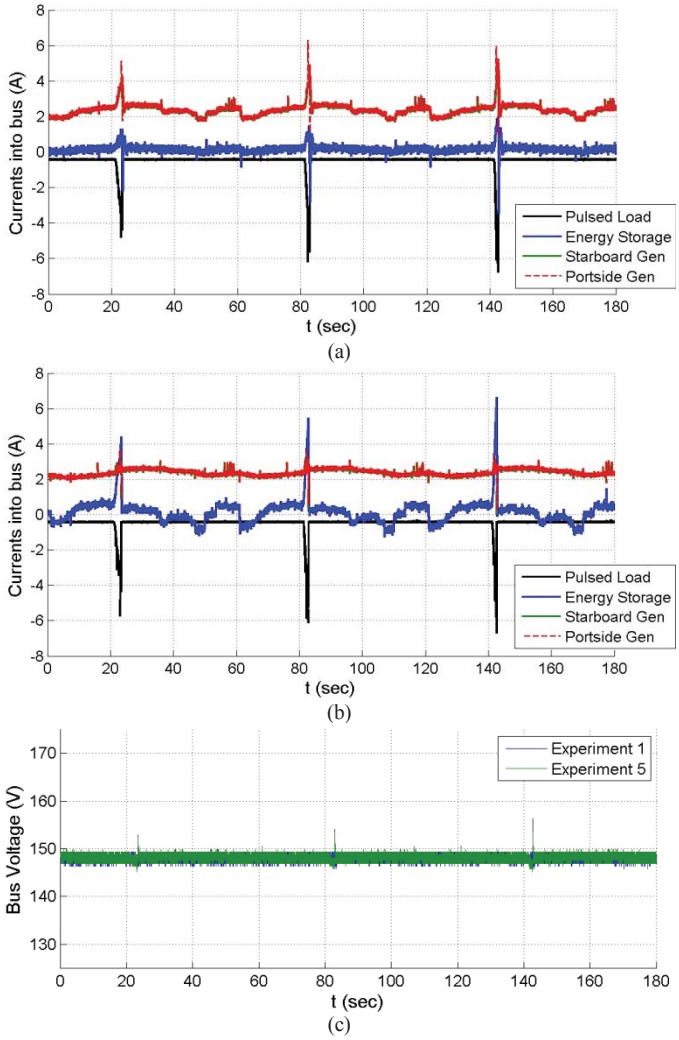

Fig. 12. Measured bus currents for (a) Experiment 1 and (b) Experiment 5 and (c) bus voltages for each

The resulting Pareto frontier obtained from the hardware experiment, comparing control effort cost from the two generators and one energy storage emulator, is shown in Fig. 14. The hardware results are intuitive and consistent with simulation; the Pareto frontier for the two cost measures shows a clear trade-off with an almost linear frontier.

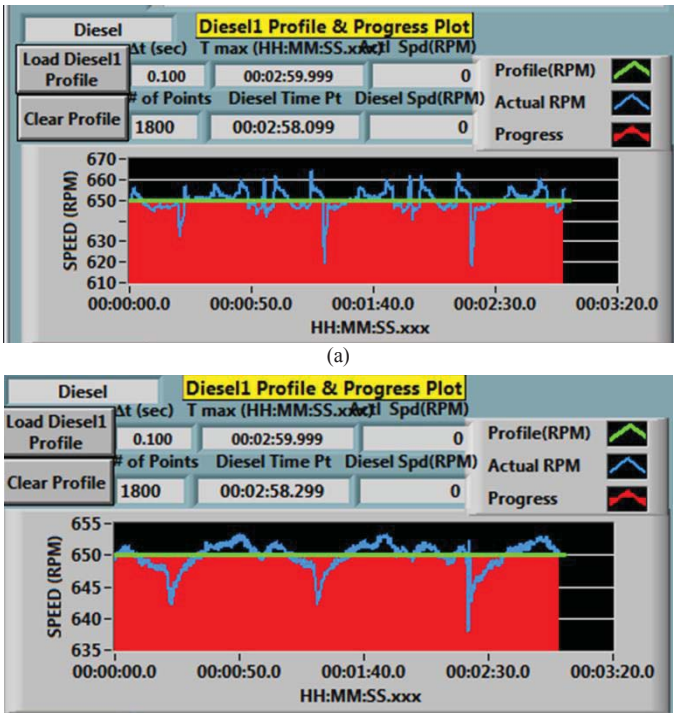

Fig. 13. Shows master control console close-up of the generator 1 speed deviations relative to the reference for (a) Experiment 1 and (b) Experiment 5.

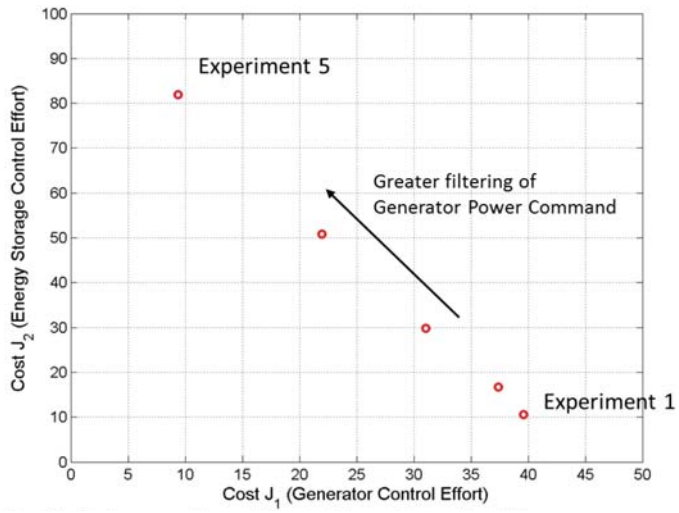

Fig. 14. Trade space (Pareto Frontier) illustrating trade-off between generator control effort and energy storage control effort

VIII. Conclusions

In this paper, a hierarchical control, developed for use in networked microgrids, was applied to the problem of coordinating energy sources and energy storage onboard an all-electric ship. The problem of pulsed load management, in particular the electromagnetic launch system (EMALS), was addressed. A notional electric ship model was emulated at laboratory scale by the SSMTB, including a scaled version of an EMALS. A method of control presented in previous works [16]-[20] was modified to include a simple guidance control function for power flow control and evaluated in simulation and in hardware to mitigate disturbances caused by EMALS

power consumption during launch. This guidance control function is capable of designating where the pulsed power is supplied (energy storage units or generator inertia) through manipulation of a filter time constant. The trade-off in control effort is easily visualized and intuitive. The results suggest that the Pareto frontier may be navigated very easily by the Guidance control by simply manipulating a filter time constant rather than computationally-intensive time-domain dynamic optimization planning [20]. For systems with pulsed loads, this allows for fast on-the-fly changes to power flow control in response to dynamic time-changing priorities.

ACKNOWLEDGMENTS

This work was supported by NAVSEA for a project entitled *Nonlinear Power Flow Control Design for NGIP Energy Storage Requirements*, PR# 1400354102.

The authors wish to thank Forest White, Jazmin Pedroza, Michael Horry, Joseph Rudys, Peter Foster, and John Brown for their contributions to the hardware testbed.

Sandia National Laboratories is a multi-program laboratory managed and operated by Sandia Corporation, a wholly owned subsidiary of Lockheed Martin Corporation, for the U.S. Department of Energy's National Nuclear Security Administration under contract DE-AC04-94AL85000.

REFERENCES

[1] D. Schneider; “The Electric Warship”; IEEE Spectrum; July 2013. URL: http://spectrum.ieee.org/aerospace/military/the-electric-warship

[2] Kulkarni, S.; Santoso, S., "Impact of pulse loads on electric ship power system: With and without flywheel energy storage systems," *Electric Ship Technologies Symposium, 2009. ESTS 2009. IEEE* , pp.568-573, 20-22 April 2009.

[3] Domaschk, L.N.; Ouroua, A.; Hebner, R.E.; Bowlin, O.E.; Colson, W.B., "Coordination of Large Pulsed Loads on Future Electric Ships," *Magnetics, IEEE Transactions on* , vol.43, no.1, pp.450-455, Jan. 2007.

[4] Webb, T.W.; Kiehne, T.M.; Haag, S.T., "System-Level Thermal Management of Pulsed Loads on an All-Electric Ship," *Magnetics, IEEE Transactions on* , vol.43, no.1, pp.469-473, Jan. 2007

[5] Crider, J.M.; Sudhoff, S.D., "Reducing Impact of Pulsed Power Loads on Microgrid Power Systems," *Smart Grid, IEEE Transactions on*, vol.1, no.3, pp.270-277, Dec. 2010.

[6] Mitra, P. ; Venayagamoorthy, G.K., “An Adaptive Control Strategy for DSTATCOM Applications in an Electric Ship Power System,” *Power Electronics, IEEE Transactions on ,* vol.25, no.1, pp.95-104, Jan.2010

[7] Woodruff, S.L.; Li Qi; Sloderbeck, M.J., "Hardware-in-the-Loop Experiments on the Use of Propulsion Motors to Reduce Pulse-Load System Disturbances," *Electric Ship Technologies Symposium, 2007. ESTS '07. IEEE*, 21-23 May 2007.

[8] Salehi, V.; Mirafzal, B.; Mohammed, O., "Pulse-load effects on ship power system stability," *IECON 2010 - 36th Annual Conference on IEEE Industrial Electronics Society*, pp.3353-3358, 7-10 Nov. 2010.

[9] Doyle, M.R.; Samuel, D.J.; Conway, T.; Klimowski, R.R., "Electromagnetic aircraft launch system-EMALS," *Magnetics, IEEE Transactions on* , vol.31, no.1, pp.528-533, Jan. 1995.

[10] Steurer, M.; Andrus, M.; Langston, J.; Qi, L.; Suryanarayanan, S.; Woodruff, S.; Ribeiro, P.F., "Investigating the Impact of Pulsed Power Charging Demands on Shipboard Power Quality," *Electric Ship Technologies Symposium, 2007. ESTS '07. IEEE*, pp.315-321, 21-23 May 2007

[11] Langston, J.; Suryanarayanan, S.; Steurer, M.; Andrus, M.; Woodruff, S.; Ribeiro, P.F., "Experiences with the simulation of a notional all-electric ship integrated power system on a large-scale high-speed electromagnetic transient simulator," *Power Engineering Society General Meeting, 2006.*

[12] Balathandayuthapani, S.; Edrington, C.S.; Henry, S., "Study on converter topologies for capacitive pulse forming network and energy storage units in electric ship," *Electric Ship Technologies Symposium (ESTS), 2011 IEEE*, pp.459-462, 10-13 April 2011

[13] Jizhu Liu; Shuanghui Hao; Zili Tang; Minghui Hao, "Autonomous control of electromagnetic aircraft launch system based on decentralized architecture," *Robotics and Biomimetics, 2008. ROBIO 2008. IEEE International Conference on* , pp.2089-2092, 22-25 Feb. 2009

[14] Domaschk, L.N.; Ouroua, A.; Hebner, R.E.; Bowlin, O.E.; Colson, W.B., "Coordination of Large Pulsed Loads on Future Electric Ships," *Magnetics, IEEE Transactions on* , vol.43, no.1, pp.450-455, Jan. 2007

[15] Mitra, P.; Venayagamoorthy, G.K., "A DSTATCOM controller tuned by Particle Swarm Optimization for an Electric Ship Power System," *Power and Energy Society General Meeting - Conversion and Delivery of Electrical Energy in the 21st Century, 2008 IEEE* , pp.1-6, 20-24 July 2008

[16] Robinett, R.D.; Wilson, D.G.; Nonlinear Power Flow Control Design: Utilizing Exergy, Entropy, Static and Dynamic Stability, and Lyapunov Analysis; Springer-Verlag, London, 2011.

[17] Robinett, R.D.; Wilson, D.G.; "Nonlinear power flow control design for combined conventional and variable generation systems: Part I-theory," *Control Applications (CCA), 2011 IEEE International Conference on* , pp.61-64, 28-30 Sept. 2011.

[18] Wilson, D.G.; Robinett, R.D.; "Transient stability and performance based on nonlinear power flow control design of renewable energy systems," *Control Applications (CCA), 2011 IEEE International Conference on*, pp.881-886, 28-30 Sept. 2011.

[19] Wilson D. G., Robinett III R. D., Goldsmith S. Y. “Renewable energy microgrid control with energy storage integration,” *International Symposium on Power Electronics, Electrical Drives, Automation and Motion (SPEEDAM)*, June 20th-22nd, 2012, Sorrento, Italy.

[20] Wilson, D.G.; Neely, J.C.; Cook, M.A.; Glover, S.F.; Young, J.; Robinett, R.D., "Hamiltonian control design for DC microgrids with stochastic sources and loads with applications," *Power Electronics, Electrical Drives, Automation and Motion (SPEEDAM), 2014 International Symposium on* , pp.1264-1271, 18-20 June 2014.

[21] S. Glover, J. Neely, A. Lentine, J. Finn, F. White, P. Foster, O. Wasynczuk, S. Pekarek, B. Loop, “Secure Scalable Microgrid Test Bed at Sandia National Laboratories,” IEEE Cyber 2012 Conference, May 27th-31st, 2012, Bangkok, Thailand.

[22] J. Neely, S. Pekarek, S. Glover, J. Finn, O. Wasynczuk, and B. Loop, “An economical diesel engine emulator for micro-grid research,” *International Symposium on Power Electronics, Electrical Drives, Automation and Motion (SPEEDAM)*, June 20th-22nd, 2012, Sorrento, Italy.

[23] J. Neely, S. Glover, O. Wasynczuk, B. Loop, “Wind turbine emulation for intelligent microgrid development,” IEEE Cyber 2012 Conference, May 27th-31st, 2012, Bangkok, Thailand.

[24] Doyle, Michael R.; Samuel, Douglas J.; Conway, Thomas; Klimowski, Robert R; “Electromagnetic Aircraft Launch System – EMALS,” *IEEE Transactions on Magnetics,* Vol. 31, No. 1, January, 1995.

[25] URL: https://en.wikipedia.org/wiki/McDonnell_Douglas_F/A-18_Hornet

[26] URL: https://en.wikipedia.org/wiki/Lockheed_Martin_F-35_Lightning_II

[27] Weaver, W.W., Robinett III, R.D., Parker, G.G., and Wilson, D.G., Distributed Control and Energy Storage Requirements of Networked DC Microgrids, Control Engineering Practice 44 (2015), pg.10-19,June 2015.